Nonlinear Saturation and Recurrence of the Two-Plasmon Decay Instability

A. Bruce Langdon, Barbara F. Lasinski, and William L. Kruer
Lawrence Livermore Laboratory, University of California, Livermore, California 94550
(Received 12 February 1979)

Two-dimensional computer simulations show that short-wavelength ion fluctuations and density-profile steepening are dominant factors in the saturation of the $2\omega_{pe}$ instability. The long-term evolution of this instability is described and the implications of this complex saturation process for absorption and harmonic emission are discussed.

Nonlinear saturation mechanisms of high-frequency instabilities which occur at or below quarter-critical density in laser-plasma interactions are currently of experimental interest.[1-4] Increasing evidence for a high-energy electron component[5] has focused attention on these instabilities which include the $2\omega_{pe}$ process, the decay of the incident electromagnetic wave into two plasma waves, and stimulated Raman scattering (SRS), in which the incident light decays into an electromagnetic wave and a plasma wave. We have simulated this density region using the computer model ZOHAR[6] and find that ion dynamics determines the saturation of these high-frequency instabilities over a large parameter range.

To make connection to previous work,[6,7] we describe briefly case A, a simulation with the ion motion frozen and parameter choices guided by laser-plasma interaction experiments with an Nd:glass laser. The simulation system consists of a plasma slab with a linear density gradient in the x or open-sided direction and periodic in the y direction. The light, normally incident from the left, produces an oscillatory velocity, $v_0 = 0.1c$ (10^{16} W/cm^2 for Nd:glass). The background electron temperature is 1 keV and the density-gradient scale length corresponds to 25 vacuum wavelengths (λ_0) from vacuum to critical density (ρ_c). The $2\omega_{pe}$ instability occurs first with a growth rate of $0.01\omega_0$, approximately half the maximum[8] $\frac{1}{4}k_0 v_0$ (Fig. 1, A). Modes 3 and 4 ($k_y \sim k_0$) are the most unstable, as predicted by theory.[9] For these parameters, $k_0\lambda_{De} \gtrsim 0.1$, and higher electron plasma wave numbers are limited by Landau damping. Raman backscattering has slower growth as a result of its higher gradient threshold,[10] and emerges after $650\omega_0^{-1}$. For this restricted problem, saturation is due to electron trapping with ~20% absorption into a 70-keV Maxwellian [$\ln f(E) \propto -E/(70$ keV) out to 450 keV].

Before SRS dominates the simulation, the $2\omega_{pe}$ peak decay-wave oscillation velocity is greater than 5 times the thermal velocity. Therefore, ponderomotive forces exceed thermal forces and ion motion must be included. Case B incorporates the ion motion into case A with $m_i/m_e = 3600$ and $ZT_e/T_i = 4$. Initial growth is the same, but initial saturation occurs below the level reached in case A at the same time (Fig. 1, B). Large-amplitude ion fluctuations, driven up by the ponderomotive forces from the electron plasma waves and concentrated just below the quarter-critical region with both x- and y-dependent variation (Fig. 2), arrest the growth of the $2\omega_{pe}$ decay waves by coupling them to short-wavelength, more strongly damped fluctuations.[11] The largest ion fluctuations.[11] The largest ion fluctuation is in mode 6 ($k_y = 1.8k_0$), $\delta n/n$ reaching

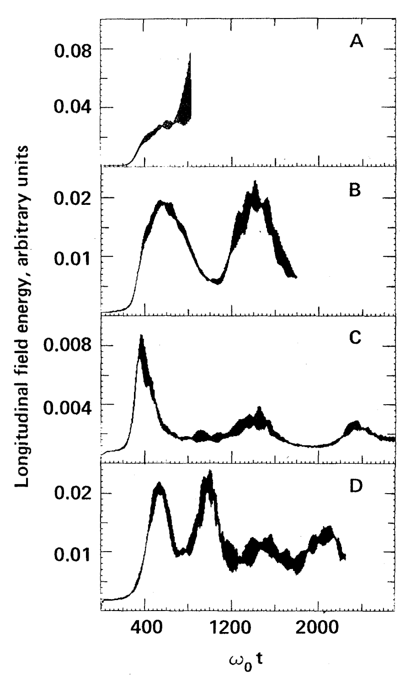

FIG. 1. Longitudinal-field energy vs time for four simulations with $v_0 = 0.1c$ and density-gradient scale length $25\lambda_0$. Case A has $T_e = 1$ keV and immobile ions; B has $T_e = 1$ keV, $m_i/m_e = 3600$, and $ZT_e/T_i = 4$; C has $T_e = 1$ keV, $m_i/m_e = 100$, and $ZT_e/T_i = 4$; D has $T_e = 10$ keV, $m_i/m_e = 100$, and $ZT_e/T_i = 4$.

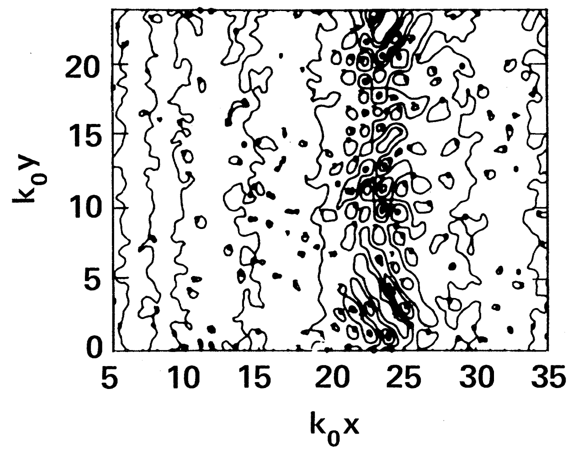

FIG. 2. Ion density contours for the simulation of case B, Fig. 1, at initial saturation, $\omega_0 t = 600$. The quarter-critical surface is at $k_0 x = 26$ and the contours are $0.03\rho_c$ apart.

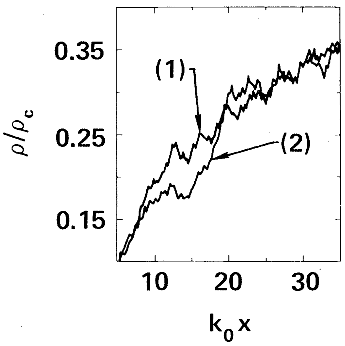

FIG. 3. Density averaged over y from a simulation similar to case C, Fig. 1, but with $ZT_e/T_i = 1$. Curve 1 is the profile at initial saturation, $\omega_0 t = 360$, and curve 2 is at $\omega_0 t = 750$.

~ 20%.

This process is reminiscent of the oscillating two-stream instability and plasmon + phonon decay with finite-wavelength pump, but is simpler in that several plasma waves with low-frequency beats already exist. That is, the parametric instability feedback mechanism, in which the beating plasma waves are driven up by the ion perturbation and the pump, is unnecessary and the ion fluctuations here grow more immediately.

Simple estimates clarify the saturation mechanism. A standing plasma wave (k, ω) produces an ion perturbation δn at $2k$, which in turn couples it to a heavily damped plasma fluctuation at $3k$. Equating the resulting damping rate[11] to the instability growth rate predicts $\delta n/n \sim \frac{1}{2}$, which is within a factor of 2 of the observed value. Using two coupled equations for wave energy and density fluctuation, we find ion inertia essential to model the relaxation behavior.

At initial saturation, the density profile shows negligible change. However, an outward impulse has been delivered to the ions causing a density depression to form which then evolves into a density step as the plasma below quarter-critical expands and blows off. We have not attempted to run a realistic mass-ratio simulation long enough to observe profile steepening. To study this later evolution, we use an ion-to-electron mass ratio that is artificially low but still separates the electron and ion time scales. For case C, similar to B but with $m_i/m_e = 100$, initial saturation occurs earlier and at a lower level (Fig. 1, C). The profile then steepens to $L \sim 5\lambda_0$, sufficient to stabilize the instability.[9] To present easily visible profiles in Fig. 3, the y-averaged density at initial saturation ($\omega_0 t = 360$) and the subsequently steepened profile ($\omega_0 t = 750$) are from a simulation similar to case C except that $T_i = T_e$ to minimize the everpresent Brillouin scattering in the plot. Nonetheless, the high-frequency instabilities and the profile do have the same behavior as functions of time in case C and its $T_i = T_e$ variant.

This steepened profile then inhibits the high-frequency instabilities, even after the short-wavelength ion turbulence subsides. Eventually the profile relaxes and the instabilities recur. As another example of the electrostatic energy as a function of time, a low-mass-ratio simulation with 10-keV electron background (case D) is shown in Fig. 1, D. Differences such as the increased electron thermal pressure, which resists the ion response, preclude comparison of the magnitude of the electrostatic energy in D with respect to C. For the parameter range we have considered, the peak longitudinal-field energy and the time between bursts of varying clarity differ, but the qualitative description holds.

Direct experimental evidence consistent with this complex saturation mechanism has been observed in CO_2-laser–plasma interaction experiments by Baldis, Samson, and Corkum.[1] They report profile steepening by a factor of 3 through the quarter-critical region as the $2\omega_{pe}$ instability turns off. Also, they observe enhanced ion fluctuations which may be identified with those described here.

Since the importance of density profile modification to the $2\omega_{pe}$ instability was first reported,[6] a theoretical description in terms of solitons has been proposed.[12] Our low-mass-ratio simulations easily satisfy the condition given for validity of the theory, $v_0/c \ll 5(m_e/m_i)^{1/2}$. If we apply Eqs. (15) through (16) of Ref. 12 to case C, the predictions are too small. Their $v_w/v_{\rm th}$ is 0.7 vs ~3 at initial saturation and their density fluctuation is 2% compared to 25% for the highest mode at $\omega_0 t = 400$. Furthermore, the absorption is 0.025% as against ~1% in this simulation.

Even qualitatively, the soliton approach assigns the ions too limited a role. Because Ref. 12 includes only a single decay pair and averages over the short-wavelength beat, the driving force for the ion fluctuations responsible for saturation is omitted. These ion fluctuations are two dimensional as opposed to the ion perturbation in Ref. 12 which depends only on x, the density-gradient direction. The theory envisions decay plasmons always self-trapped in local density depressions given by the hydrostatic response to the ponderomotive pressure of the decay waves. In the simulations, the decay plasmons have already been damped before a density depression forms. When the $2\omega_{pe}$ instability resumes, the ion density (averaged over y) has become monotonic in x, thereby excluding plasmon trapping. Even in small-mass-ratio simulations, ion inertia causes obvious delays and overshoots in the ion response at both short and long wavelengths.

We now discuss the implications of $2\omega_{pe}$ saturation for some recent experiments.[13] We use case D, the simulation with the 10-keV background temperature, on the assumption that heating at critical density is flooding the quarter-critical region with hot electrons.[13] Whereas steepening at critical density enhances resonance absorption, steepening at quarter-critical limits the $2\omega_{pe}$ and Raman instabilities. Absorption (averaged over instability bursts and quiescent interim periods) is 6% in case D. (Absorptions of 1 to 10% encompass other simulation results.)

Electron heating, correlated with these recurrences, results in a 75-keV Maxwellian out to 450 keV. This is somewhat hotter than the spectrum produced by resonance absorption for the same simulation conditions.[14] However, this result needs qualification. 30% of the electron energy is above 0.5 MeV in a 10-keV simulation with the pump incident at 40° and with particle boundary conditions which model suprathermal reheating. Above 10 keV, Landau damping limits heating from the $2\omega_{pe}$ and Raman instabilities at 10^{16} W/cm^2, although "hot spots" in the beam or filamentation may produce local, discrete regions of intensity large enough to overcome plasma-wave damping.[4] Experimentally, high-energy electrons appear when plasma conditions are hospitable to parametric instabilities.[2]

The emission of $3\omega_0/2$ light has long been used as a diagnostic of the quarter-critical surface.[3] In our simulations, both $3\omega_0/2$ and $\omega_0/2$ emission occur at low levels. For case D, 1% of the incident power emerges as $\omega_0/2$ light, peaked at a slab exit angle of 31°. Less than 0.1% of the incident power is in $3\omega_0/2$ emission. However, these fractions do not imply that SRS is dominating the $2\omega_{pe}$ process. Raman scattering produces $\omega_0/2$ light directly, while $3\omega_0/2$ light is a subsequent combination of a decay plasma wave and a light wave at ω_0, or higher-order combinations, e.g., of three plasma waves. If SRS were dominant, then the energy in the heated-particle distribution should at least equal the energy produced in $\omega_0/2$ light. Even if we assume that half of this $\omega_0/2$ light is resonantly absorbed at its critical surface, there is still not enough $\omega_0/2$ light emitted. Also, self-steepening through the quarter-critical region limits SRS more than the $2\omega_{pe}$ instability.[8-10] Another possibility is that the $2\omega_{pe}$ decay plasma waves at $\omega_0/2$ couple to electromagnetic waves by tunneling, a process which may be thought of as inverse to resonance absorption.

Thus, simulations indicate that the $2\omega_{pe}$ instability is probably dominant near quarter critical. Important components in the saturation are damping by short-wavelength ion fluctuations and profile self-steepening. The $2\omega_{pe}$ instability exhibits relaxation behavior which limits its efficiency as a light-absorption mechanism and affects its experimental signatures.

This work was performed under the auspices of the U. S. Department of Energy by the Lawrence Livermore Laboratory under Contract No. W-7405-ENG-48.

[1]H. A. Baldis, J. C. Samson, and P. B. Corkum, Phys. Rev. Lett. 41, 1719 (1978).

[2]C. M. Armstrong *et al.*, U. S. Naval Research Laboratories report (to be published); K. G. Tirsell and H. C. Catron, Lawrence Livermore Laboratory Report No. UCRL-80322, 1977 (unpublished).

[3]A. A. Offenberger *et al.*, Phys. Rev. A 18, (1978); S. Jackel, J. Albritton, and E. Goldman, Phys. Rev. Lett. 35, 514 (1975).

[4]T. A. Leonard and R. A. Cover, J. Appl. Phys. 50, 3241 (1979); M. H. Key *et al.*, Rutherford Laboratory

Report No. LD/78/01 (unpublished).

[5]G. McCall, private communication.

[6]A. B. Langdon and B. F. Lasinski, in Fusion Research, edited by J. Killeen, Vol. 16 of Methods in Computational Physics, edited by B. Alder, and S. Fernbach, and M. Rotenberg (Academic, New York, 1976), p. 327.

[7]D. Biskamp and H. Welter, Phys. Rev. Lett. 34, 312 (1975).

[8]C. S. Liu and M. N. Rosenbluth, Phys. Fluids 19, 967 (1976).

[9]B. F. Lasinski and A. B. Langdon, Bull. Am. Phys. Soc. 22, 1174 (1977), and to be published.

[10]C. S. Liu, M. N. Rosenbluth, and R. B. White, Phys. Fluids 17, 1211 (1974); H. H. Klein, W. M. Manheimer, and E. Ott, Phys. Rev. Lett. 31, 1187 (1973); J. F. Drake and Y. C. Lee, Phys. Rev. Lett. 31, 1197 (1973).

[11]J. M. Dawson and C. Oberman, Phys. Fluids 6, 394 (1963).

[12]H. H. Chen and C. S. Liu, Phys. Rev. Lett. 39, 881 (1977).

[13]M. D. Rosen *et al.*, Lawrence Livermore Laboratory Report No. UCRL-80862, 1978, and to be published.

[14]K. Estabrook and W. L. Kruer, Phys. Rev. Lett. 40, 42 (1978); D. W. Forslund, J. M. Kindel, and K. Lee, Phys. Rev. Lett. 39, 284 (1977).

Structure Functions of Quenched Off-Critical Binary Mixtures and Renormalizations of Mobilities

Hiroshi Furukawa

Department of Physical Sciences, Faculty of Education, Yamaguchi University, Yamaguchi 753, Japan

(Received 14 May 1979)

Structure functions of quenched off-critical binary mixtures are studied from a unified viewpoint. Individual systems are characterized only by the properties of their mobilities. The comparisons of theoretical predictions with experiments on the kinetic Ising spin model, binary fluid mixtures, and alloys yield with good agreement.

The phase separation of a binary mixture proceeds accompanied by cluster coagulations. A state where clusters are formed is represented by a local minimum of the free energy at which the first derivative of the free energy should vanish. The free energy thus contains an infinitely large number of local minima characterized by cluster sizes and cluster configurations. If the phase separation of a quenched binary mixture proceeds into a completely phase-separated state only through the local minima of the free energy, then the restoring forces acting on fluctuations with wave numbers smaller than the inverse cluster diameter should always be vanishingly small. For off-critical quenchings two further simplifications can be found. First, the fluctuations inside clusters can be neglected and therefore the restoring forces acting on fluctuations with wave numbers larger than the inverse cluster diameter are extremely large. Second, the length scale is the average cluster diameter R, only. Therefore, the structure function $S_k(t)$ may be scaled as

$$S_k(t) = R^d \tilde{S}(kR), \qquad (1)$$

where d is the dimensionality. On the basis of these ideas we have derived the equation of the motion for $S_k(t)$ in the case of off-critical quenching[1] and obtained a good agreement with computer simulations on the spin-exchange kinetic Ising spin model.[2,3] Nevertheless, there remains an ambiguity in determining the R dependence of the mobility, i.e., the renormalization of the mobility is not yet considered. This is the reason why our previous discussion failed to explain other cases, e.g., the off-critical quenching of a binary fluid mixture.[4] In this short communication the renormalization of the mobility will be considered with the help of the cluster dynamics due to Binder and Stauffer.[5]

Consider the following Langevin-type equation for the composition fluctuation $\eta_k(t)$, which is the Fourier component of the local composition $\eta(t,r)$:

$$\frac{d}{dt}\eta_k = -\Gamma_k(t)\eta_k(t) + g_k(t), \quad \langle g_k(t)\eta_k{}^*\rangle_0 = 0; \qquad (2)$$

$$\langle g_k(t) g_k{}^*(s)\rangle_0 = 2k_B TM(t)k^2\delta(t-s), \qquad (3)$$

where $M(t)$ is the renormalized mobility, k_B is Boltzmann's constant, T is the temperature, B is a constant, and $\langle\rangle_0$ means the ensemble average in a state observed. Then the damping coefficient $\Gamma_k(t)$ may be approximately given, for the reason mentioned above, by

$$[k_B TM(t)k^2]^{-1}\Gamma_k(t) \equiv \chi_k{}^{-1}(t) = B^{-1}R^{-d}(kR)^{d+1}. \quad (4)$$